October 2020

On the Stress Concentration at Sharp V-Notches Under Tension

Trent Mattieu Andrus
Louisiana State University and Agricultural and Mechanical College

ON THE STRESS CONCENTRATION AT SHARP V-NOTCHES UNDER TENSION

A Thesis

Submitted to the Graduate Faculty of the
Louisiana State University and
Agricultural and Mechanical College
in partial fulfillment of the
requirements for the degree of
Master of Science

in

The Department of Mechanical and Industrial Engineering

by
Trent Mattieu Andrus
B.S., Louisiana State University, 2018
December 2020

Acknowledgments

It is with deep gratitude that I extend a thank-you to my advisor and mentor, Dr. Glenn B. Sinclair. Throughout this research, I have grown academically and personally, guided by your expertise, exacting standards, support, and willingness to teach. This research was deeply engaging and challenging. I am thankful for the opportunity to contribute to this body of engineering knowledge in a meaningful way with your guidance. Moreover, you provided me an avenue to realize my professional aspirations, for which I am eternally grateful.

I also extend a thank-you to my colleagues at Ansys: Roxana Cisloiu, Jeff Beisheim, and Krishna Trikutam. Through your guidance and patience, I gained new, significant insights to the ANSYS software and best practices that I applied immediately and directly to my research.

To my family: there are innumerable things for which I am deeply grateful. In this venture, I thank my parents, Mattieu and Claire, for their emotional and financial support. You provided space for me to air my excitements, my grievances, and everything in-between. The completion of this work is a culmination of my interests and work ethic that you have fostered in me throughout my lifetime. I thank my siblings, Seth and Camille, for providing a much-needed distraction at times, be it a deeply engaging conversation or uncontrollable late-night laughter. My family's support was instrumental in my success in this, and other, commitments.

Finally, to my fiancée, Madelyn Smith, words cannot express my gratitude for everything you do. You provide endless support and encouragement. Thank you for pushing me to pursue an advanced degree and challenge myself in this way. Thank you for your patience over many years of continuous work and the sacrifices that accompanied that work. I look forward to sharing more of life's pleasures with you.

Table of Contents

Acknowledgments....ii

Abstract....iv

1. Introduction....1

2. Problem Formulation....3

3. Finite Element Analysis and Verification....9

4. Results for Peak Notch Stresses....13

5. Concluding Remarks....22

Appendix A. Finite Element Meshes....23

Appendix B. Fields for Tuned Test Problems....27

Appendix C. Convergence Checks for Maximum Stresses with Uniform Cohesive Laws....28

Appendix D. Convergence Checks for Maximum Stresses with Cohesive Laws on Symmetry Plane....31

Appendix E. Peak Stress Results with r_o=0 with Cohesive Laws on the Symmetry Plane....33

References....35

Vita....36

Abstract

Accurately determining stresses at re-entrant corners using finite element analysis (FEA) is challenging due to the high stresses produced at the corner. Indeed, FEA is unable to obtain quantitatively accurate peak stresses at mathematically sharp re-entrant corners with traditional boundary conditions because these stresses are singular. Imposing a local corner radius by rounding the sharp corner to remove the singular result is an appropriate technique for large radii, but as the corner radius tends to zero and the notch is close to being sharp, we expect there are radii that yield quantitatively inaccurate results with traditional FEA. We seek to determine a range of radii that are solved accurately with traditional boundary conditions and determine a finite stress result for a sharp re-entrant corner.

Here, we improve upon traditional boundary conditions by employing cohesive stress-separation laws in an elastic plate for a series of 90-degree V-notches with radii. We use convergence checks and construct test problems to verify our FEA. Then, we determine a range of radii for which traditional FEA is appropriate and accurate. Further, we obtain results for radii which are beyond the applicability of traditional FEA.

Through our analysis, we find that traditional FEA is appropriate for a broad range of notch radii. In addition, we find that the maximum peak stress does not occur for a sharp corner, but rather for a V-notch with a small radius.

1. Introduction

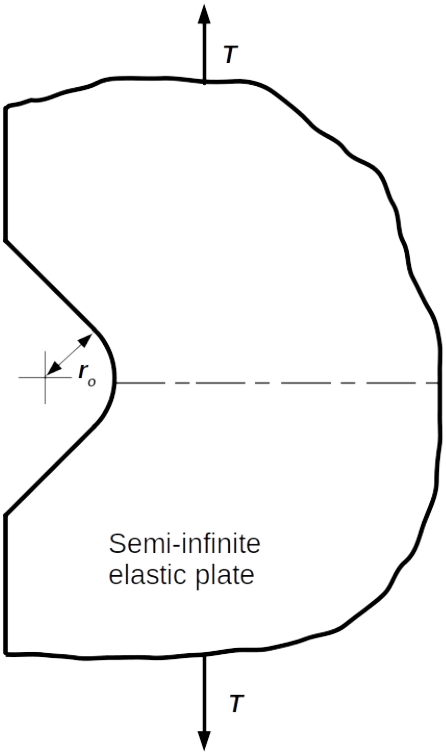

Fig. 1. Plate with V-notch under tensile loading

The geometry of interest is shown in Fig. 1, which has a semi-elastic infinite plate under tensile loading *T*, with a 90-degree V-notch that has a local notch radius r_o, also referred to as a re-entrant corner. The notch radius acts as a stress concentrator, increasing local stresses significantly as the radius decreases in size. We are most interested in the peak stress at the notch as r_o approaches zero, which is the case of a mathematically sharp 90-degree V-notch.

Williams [1] determined an asymptotic solution for the stresses at a sharp re-entrant corner under transverse tension with traditional symmetry conditions on the midplane. However, this solution yields a stress result that is on the order of $(1/r^{0.456})$, where *r* is the radial distance from the sharp corner. Hence, an infinite stress as *r* approaches zero. Though qualitatively correct

in reflecting the increased stress at the corner, this singular stress is quantitatively incorrect. Hence, there must be some radii near r_o=0 where the stresses are also quantitatively inaccurate with traditional symmetry conditions. Our principal intention is to determine a range of radii for which this traditional analysis is quantitatively accurate.

By introducing cohesive stress-separation laws to the notch face and midplane, it is possible to remove the singular stress result, as demonstrated in Sinclair [2]. The cohesive laws basically act as stiff springs between the upper and lower half of the plate that respond identically to the surrounding elastic solid, and finite stresses result for all values of r_o. This allows us to determine a range of radii for which traditional symmetry conditions produce the same results as cohesive laws, and so are quantitatively accurate. For those radii that do not yield the same results, we can still obtain a physically accurate theoretical solution for the maximum stress with the cohesive laws.

In this work, we parallel the analysis conducted by Sinclair et al. [3] for an elliptical crack tip in tension as crack-tip radii decrease and cohesive stress-separation laws are implemented. Results from Ref. [3] show the cohesive action reduces the peak stress for a crack to a finite value. We expect a similar trend here. Reference [3] conducts FEA and subsequent verification using test problems drawn from classical elasticity solutions, then further confirms FEA results through integral equations. Here, we too use FEA to explore the action of cohesive laws, and we verify the FEA with convergence checks and test problems that we construct.

We begin in Sec. 2 with a formal problem statement for the 90-degree V-notch and provide a simplified cohesive stress-separation law. In Sec. 3, we describe the FEA of this problem and our approaches for verification. In Sec. 4, we provide FEA results that demonstrate verification then give results for peak stresses at the notch tip.

2. Problem Formulation

We invoke symmetry to confine our attention to the upper half of the plate in Fig. 1. To enable FEA, we reduce the extent of this half-plate to a finite width W and height H (Fig. 2). We determine W and H such that the FEA results at the notch tip cease to change for larger dimensions of W and H. The finite plate is then, in effect, akin to a semi-infinite plate. The plate continues to have a V-notch with radius r_o. The notch depth is d, and the projected depth of a sharp notch is L. The region occupied by this plate is $\Re$.

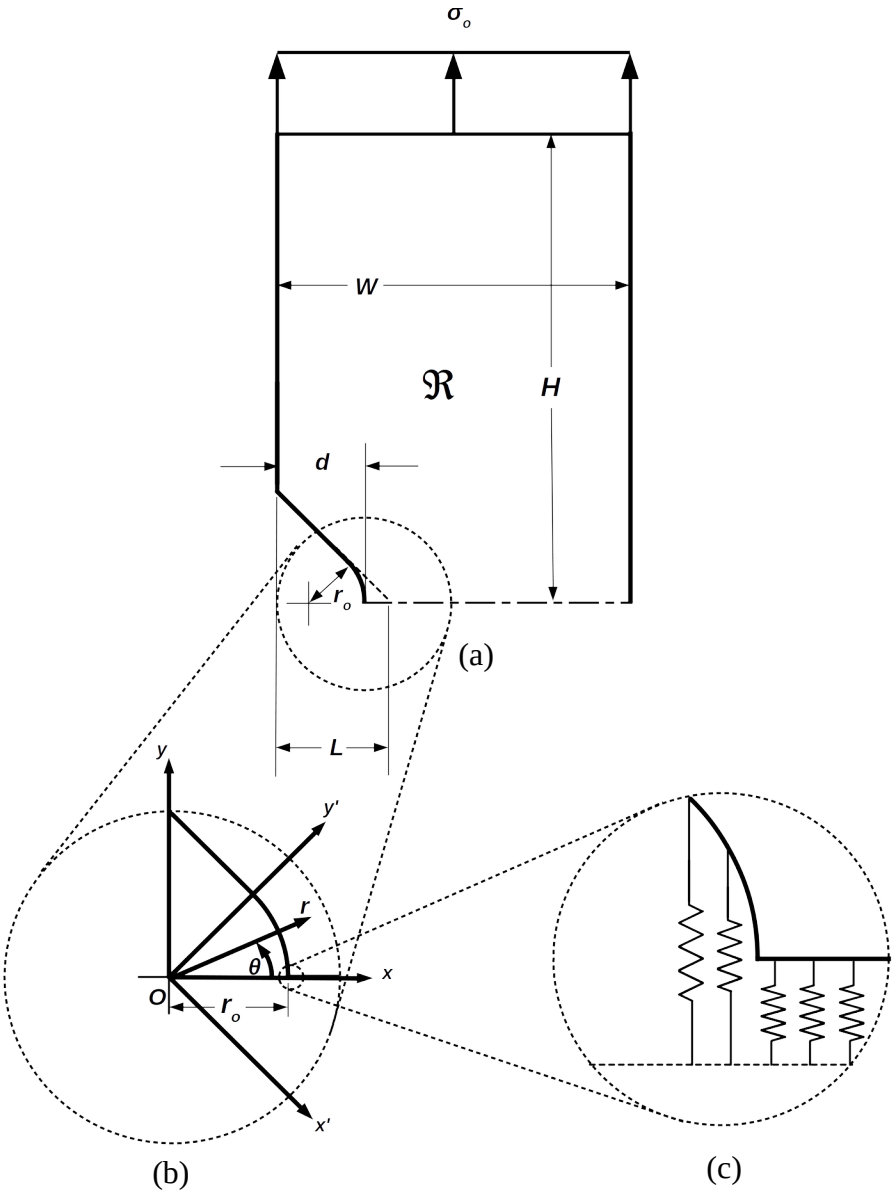

Fig. 2. Elastic V-notched plate under uniform tension: (a) geometry, (b) coordinate systems, (c) cohesive law stiffnesses

The plate is loaded by a uniform tensile traction σ_o. This loading is resisted by cohesive stresses along the base symmetry line and the notch face. Even with an underlying constant cohesive law in place, the notch face will be subject to different stiffnesses, as reflected by the springs in Fig. 2(c). The peak stresses induced by this loading at the tip of the V-notch are of paramount interest here.

The geometry of the plate is readily framed by three coordinate systems: a rectangular Cartesian system, (x, y), a cylindrical polar system, (r, θ), and a further rectangular Cartesian system, (x', y'). All three coordinate systems share a common origin O (see Fig. 2(b)). The (x, y) system and the (r, θ) system are related by

$$x = r\cos\theta, \quad y = r\sin\theta. \tag{1}$$

The (x', y') system is a rotation of (x, y) by $-\pi/4$ about the origin O, and is used to express the boundary conditions on the notch face.

In general, we seek the plane strain stresses σ_x, σ_y, and τ_{xy}, together with their companion displacements u_x and u_y throughout $\mathfrak{R}$ satisfying the appropriate two-dimensional field equations and boundary conditions as r_o tends to zero. The field equations are the stress equations of equilibrium without body forces, and the stress-displacement relations for a homogeneous, isotropic, linear, elastic solid in a state of plane strain. The boundary conditions are as follows: the loading condition,

$$\sigma_y = \sigma_o, \tau_{xy} = 0 \text{ on } y = H, \tag{2}$$

for $-(d - r_o) < x < W - (d - r_o)$; the stress-free conditions,

$$\sigma_x = \tau_{xy} = 0 \text{ on } x = -(d - r_o), x = W - (d - r_o), \tag{3}$$

for $L < y < H$, $0 < y < H$, respectively; and the cohesive stress-separation laws, along the symmetry line $y=0$,

$$\sigma_y = \sigma_c,\ \tau_{xy} = 0 \ \text{ on } \ y = 0, \tag{4}$$

for $r_o < x < W - d$, where $\sigma_c = \sigma_c(2u_y)$ is the cohesive stress-separation law, on the notch radius,

$$\sigma_r = \sigma_c \sin\theta,\ \tau_{r\theta} = \sigma_c \cos\theta \text{ on } \ r = r_o, \tag{5}$$

for $0 < \theta < \pi/4$, and along the notch flank,

$$\sigma_{y'} = \sigma_c/\sqrt{2},\ \tau_{x'y'} = \sigma_c/\sqrt{2} \text{ on } \ y' = r_o, \tag{6}$$

on $-\sqrt{2}L + r_o < x' < 0$. In particular, we seek the normalized maximum stress

$$\overline{\sigma}_{\max} = \sigma_{\max}/\sigma_o, \tag{7}$$

at the notch root, where $\sigma_{\max} = \sigma_y$ at $x = r_o$, $y = 0$.

There are two comments regarding the foregoing formulation. First, the factor of two in the argument of $\sigma_c = \sigma_c(2u_y)$ occurs because the total separation of the upper and lower plate portions in Fig. 1 is twice that of the separation of only the upper portion from the symmetry line $y = 0$. Second, because of the symmetry of the configuration, there is no horizontal force induced in any of the cohesive stress separation laws in Eqs. (4)–(6).

Concerning the cohesive stress-separation law, Fig. 3 shows the simplified law adopted here to approximate the cohesive stress σ_c induced between two elastic half-spaces as the separation s increases above its equilibrium value δ. This law consists of an initial linear segment, then a plateau at the theoretical ultimate stress σ_U, then a decrease through a transitional linear segment which smoothly joins the response for large separations, which is $O(s^{-3})$. More precisely,

$$\begin{aligned}
\sigma_c &= \kappa s \quad (s \le s_U), \\
\sigma_c &= \sigma_U \quad (s_U \le s \le 2s_U), \\
\sigma_c &= \sigma_U - \kappa'(s - 2s_U) \quad (2s_U \le s \le s_i), \\
\sigma_c &= \sigma_U C/s^3 \quad (s_i \le s \le s_o).
\end{aligned} \tag{8}$$

In Eq. (8), κ is the initial stiffness per unit area, s_U is the separation at which the theoretical ultimate stress σ_U is obtained, s_i is the inner separation and s_o an outer separation (not shown in Fig. 3), κ' is the transitional stiffness per unit area, and C is a constant.

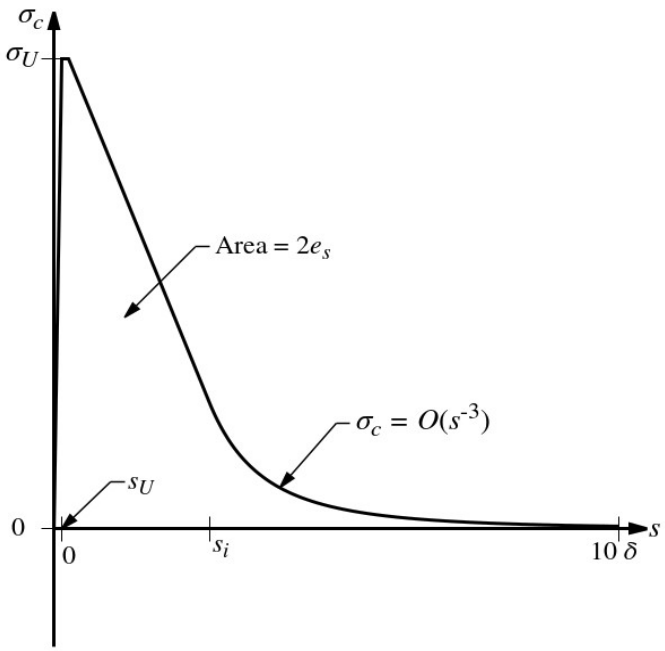

Fig. 3. Cohesive stress-separation law

This law is the same as in Ref. [3], including the determination of the aforementioned parameters, with three key points concerning the parameters addressed here. First, in Ref. [3], the initial stiffness per unit area, κ, is determined by applying the cohesive law to a uniaxial tensile specimen and ensuring that the specimen's response with the cohesive law is identical to the specimen's response without the cohesive law. This leads to

$$\kappa = \frac{2\mu}{(1-\nu)\delta}, \tag{9}$$

where μ is the shear modulus and ν is Poisson's ratio. Second, Ref. [3] selects the inner transition separation s_i and the constants C and κ' to match the transitional linear segment and the large separation response in slope and magnitude at $s=s_i$, and to satisfy the energy balance

$$\int_{\delta}^{s_o} \sigma_c(s)\,\mathrm{d}s = 2e_s, \tag{10}$$

where e_s is the surface energy for each of the two new surfaces formed on complete separation. Third, Ref. [3] selects an outer separation s_o so that the cohesive stress values are reduced to a magnitude that may be considered negligible.

We use the same specific material properties as in Ref. [3]. These are for glass and are largely drawn from Cherepanov [4]. Thus, we have

$$\mu=25\ \text{GPa},\ \ \nu=0.28,\ \ \sigma_U=\frac{4\mu}{15(1-\nu)}, \tag{11}$$

from which s_U is determined to be $s_U=2/15\,\delta$. The molecular diameter for glass is used to approximate the equilibrium separation, so from Ref. [4] $\delta=0.23\,\text{nm}$. The surface energy for the glass in Ref. [4] is e_s=2.3 N/m. Reference [3] chooses s_o so that the cohesive stress at the separation s_o is reduced to approximately atmospheric pressure, which yields the transitional stiffness per unit area $\kappa'=2\kappa/51$, the separation values $s_i=11\delta/4$, $s_o=80\delta$, and the constant $C=55s_i^3/204$.

We take an initial notch size as r_o/L=1/32 and decrease the notch radius following

$$r_o/L=0.5/16^n, \tag{12}$$

for n=1, 2, 3, 4, 5. Our primary focus is on results with small values of r_o, so we introduce a further expression r_o/δ after n=5 to set these sharp notches:

$$r_o/\delta=131.6/2^p, \tag{13}$$

where p=1, 2, …, 8. This leads to r_o/δ beginning at 65.8, and halves with each increase of p until r_o/δ=0.514. Taking p=–2 in Eq. (13) represents the same configuration as taking n=5 in Eq. (12). Thus, in essence, with Eq. (13) we have defined L=254 mm (10 inches).

To this point, we have focused on results due to a uniformly applied cohesive law. However, cohesive energetics may diminish the cohesive law on the notch face. As a limiting case, we remove the law on the notch face completely, thus setting an upper bound on such effects. We restate Eqs. (5) and (6) to impose stress-free conditions: on the notch radius,

$$\sigma_r = 0, \tau_{r\theta} = 0 \text{ on } r = r_o, \tag{14}$$

for $0 < \theta < \pi/4$, and along the notch flank,

$$\sigma_{y'} = 0, \tau_{x'y'} = 0 \text{ on } y' = r_o, \tag{15}$$

on $-\sqrt{2}L + r_o < x' < 0$. With these conditions, stresses are expected to be higher as r_o approaches zero, though still finite. To track these increased stresses, we further reduce r_o with additional values for p in Eq. (13), where p=11, 12, …, 15. Guided by our results for the notches of Eqs. (12) and (13), we supplement two additional notches, r_o/δ=500 and r_o/δ=30, and obtain results for these two as well.

As an additional case, we also consider traditional symmetry conditions on y=0 and stress-free conditions on the notch face. These conditions can be expected to promote higher stress concentrations than with cohesive stresses, and so we use them in Sec. 3 for verifying our FEA. In effect, these conditions set κ in the cohesive law, Eq. (8), equal to infinity. We maintain the stress-free conditions in Eqs. (14) and (15), and divide the cohesive law through by κ, thus resulting in

$$u_y = 0, \tau_{xy} = 0, \text{ on } y = 0, \tag{16}$$

along the symmetry line for $r_o < x < W - d$.

3. Finite Element Analysis and Verification

To conduct our FEA, we use four-node quadrilateral (4Q) elements (PLANE182, Ref. [5]), and nonlinear spring elements (COMBIN39, Ref. [5]) to implement our cohesive laws. Lower-order elements are chosen in favor of higher-order elements, as higher-order elements tend to produce oscillatory results when used with nonlinear spring elements. In an effort to reduce numerical noise, we insert small cubic splines into the simplified cohesive law of Eq. (8) to round the corners, in the regions where $s=s_U \pm s_U/5$ and $s=2s_U \pm s_U/5$.

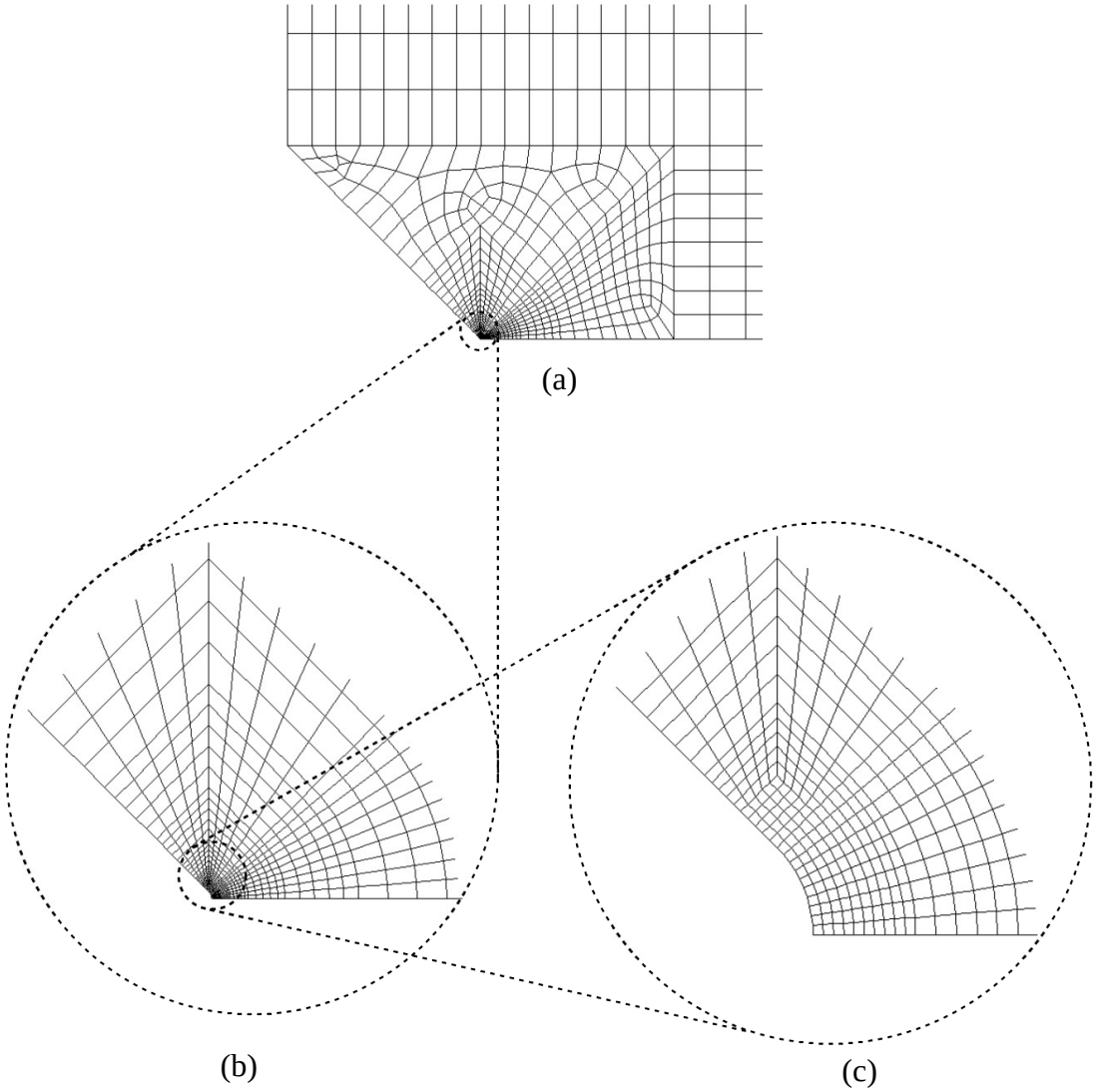

Fig. 4. Finite element mesh (m=1) for r_o/δ=65.8: (a) farfield mesh , (b) structured mesh close-up, (c) detail near notch tip

We begin our FEA with a coarse mesh that is structured near the notch face so that the elements near $x=r_o$, $y=0$ are close to square. Figure 4(a) shows the coarse mesh for r_o/δ =65.8. This configuration is selected as a representative case for several reasons. Namely, all of the more acute notch radii share exactly the same mesh structure at the notch root (Fig. 4(c)). Additionally, the structured mesh pattern that repeats itself away from the notch root (see pattern structure in Fig. 4(b)) is very similar for the more acute notches. The interior structured mesh expands away from the notch until it reaches a transition region, visible in Fig. 4(a), which connects to a structured mesh in the farfield of the plate.

In order to set the finite dimensions W and H, we first initialize these dimensions as $W=2L$ and $H=L$. The projected depth of the sharp notch L remains fixed. We then double the width of the plate until a further increase does not alter the FEA result for the maximum stress at the notch root $x=r_o$, $y=0$ to five figures. The width may be doubled by either the dimension W or the net-section width along $y=0$, which is $W-d$. We choose the latter. The magnitude of d is

$$d=L-\left(\sqrt{2}-1\right)r_o. \tag{17}$$

As the radius r_o gets small, its influence on the magnitude of d reduces and d approaches L. Upon finding an adequate width, we then double the height of the plate until the FEA result is not changing to five figures. This method establishes the farfield plate dimensions such that the result is essentially the same as for an infinite plate. We conduct this procedure for $r_o/L=1/32$ and continue the process for subsequent configurations to determine that the following dimensions, in terms of r_o and L, are appropriate for all configurations:

$$\frac{W}{L}=5+3\left(\sqrt{2}-1\right)\frac{r_o}{L},\ \ \frac{H}{L}=8. \tag{18}$$

The dimensions in Eq. (18) are simply a net-section width increase by a factor of four and a height increase by a factor of eight. No subsequent increase in these dimensions effects the solution, though smaller dimensions might.

To check for convergence, we use an element refinement factor of two. We halve element extents in the structured mesh regions, strictly quadrupling the number of elements in these regions. We approximately quadruple the number of elements in the unstructured regions, so that element extents halve on average. The total number of element comes close to quadrupling, as reflected in Table 1. For r_o/δ =65.8, Table 1 shows the mesh number m, the approximate element extent h_m/r_o on $r=r_o$, and the total number of 4Q elements N_m.

Table 1. Mesh refinement sequence for r_o/δ =65.8

m	h_m/r_o	N_m
1	1/12.7	3,549
2	1/25.4	14,184
3	1/50.8	56,666
4	1/102	226,394

Mesh refinement details for all the other notch radii are given in Appendix A.

Convergence is assessed using the error estimates of Sinclair et al. [6]. Mesh refinement continues until error estimates approach 1/5 percent, at which point the notch stress is judged to be sufficiently accurately determined.

As a further means of verification, we use tuned test problems (TTP). These are constructed for the symmetry conditions, which have the highest stress concentration factors, following the process described in Sinclair et al. [7]. Upon solving an originating FEA for a given notch configuration and reaching an acceptably converged solution, we obtain the following values at at $x=r_o$, $y=0$ from the FEA and increase each by 10 percent:

$$\sigma_{\max}/\sigma_o,\ \partial\sigma_\theta/\partial r,\ \partial^2\sigma_\theta/\partial\theta^2. \tag{19}$$

We then determine the the adjustable parameters α, β, and γ from the stress fields in Ref. [7], given in Appendix B, using the following:

$$\frac{\sigma_{\max}}{\sigma_o}=2(\alpha+2\beta+\gamma),$$

$$\frac{\partial \sigma_\theta}{\partial r}=\frac{-2\sigma_o}{r_o}(\alpha+6\beta+2\gamma), \tag{20}$$

$$\frac{\partial^2 \sigma_\theta}{\partial \theta^2}=-2\sigma_o(8\beta+\gamma),$$

where the values from Eq. (19) are taken in Eq. (20). Using the displacement fields in Ref. [7], given in Appendix B, we apply displacement boundary conditions to the originating FEA at the following boundaries:

$$x=-(d-r_o), x=W-(d-r_o), \tag{21}$$

for $L < y < H$, $0 < y < H$, respectively; on

$$y=H, \tag{22}$$

for $-(d - r_o) < x < W - (d - r_o)$; and on

$$y'=r_o, \tag{23}$$

for $-\sqrt{2}+r_o<x'<0$. We maintain the conditions from Eqs. (14)–(16) as well. From the first of Eq. (20), we have a known solution for the maximum stress at $x=r_o$, $y=0$ that is approximately 10 percent larger in magnitude than the stress of the originating FEA. Thus, these TTP are slightly more difficult to solve. Therefore, if the TTP are solved accurately with the same meshes as the originating FEA, we expect this originating and easier problem to be solved accurately with the FEA.

4. Results for Peak Notch Stresses

In Sec. 3, we describe our methodology to verify that finite width and height dimensions do not result in changes to the maximum stress at the notch root. To demonstrate this process in our choice of W and H, we consider the least acute notch, $r_o/L=1/32$, and review the maximum stress at the notch root, $x=r_o$, $y=0$, as the height and width increases. We select the least acute notch because this notch has elevated stresses distributed over the largest fraction of the net-section width. As a result, this notch will require the most substantial width increases before the behavior is essentially the same as a semi-infinite plate. Consequently, we expect that the necessary width for the least acute notch will be sufficient for more acute notches.

Table 2 shows the result of the finest mesh of $r_o/L=1/32$ for the normalized maximum stress as we double the net-section width, taking it equal to $a\times(W-d)$, where $a=1, 2, 4, 8$. We initialize the width as $W=2L$, so the initial net-section is $(2L-d)$. We maintain a constant height, $H=L$. As the width increases from $a=4$ to $a=8$, the maximum normalized result is the same to six figures, so we take the net-section width as four times its initial value, leading to the expression for W/L in Eq. (18). In a similar fashion, we now double the height for this selected width. Table 3 shows the maximum normalized stress at the notch root for $r_o/L=1/32$ as the height increases, starting with $H=2L$. Upon a height increase from $H=8L$ to $16L$, the result for maximum stress at the notch root is the same to five figures. Thus, we take the height as $H=8L$, completing the specification given in Eq. (18).

Table 2. Normalized maximum stress for $r_o/L=1/32$
upon doubling net-section width ($H=L$)

a	$\overline{\sigma}_{\max}$
1	34.1967
2	28.6376
4	28.5777
8	28.5777

Table 3. Normalized maximum stress for r_o/L=1/32 upon doubling height

H/L	$\overline{\sigma}_{\max}$
2	18.6170
4	15.8783
8	15.7945
16	15.7944

We conduct the same procedure for r_o/L=1/512 and see similar behavior as the plate dimensions Table 7 increase. Upon reaching a net-section width that is four times the initial net section, the normalized maximum stress from the finest mesh is constant to five figures upon a subsequent doubling. Likewise, the upon reaching a height of H/L=8, the normalized maximum stress is constant to five figures upon doubling to H/L=16. Thus, as we construct all of the remaining, more acute notches, we take a width that is four times the initial net section and a height that is H/L=8.

We consider r_o/δ=2.06 as a representative case to review results for verification because this configuration produces the largest normalized stress at the notch root with uniformly applied cohesive laws. Figure 5(a) shows the normal stress along the symmetry line y=0. At the scale of Fig. 5(a), the results from different meshes are indistinguishable. Figure 5(b) shows the results in detail near the notch root for each FEA mesh. As the meshes refine, the results begin to overlap as they approach the same solution.

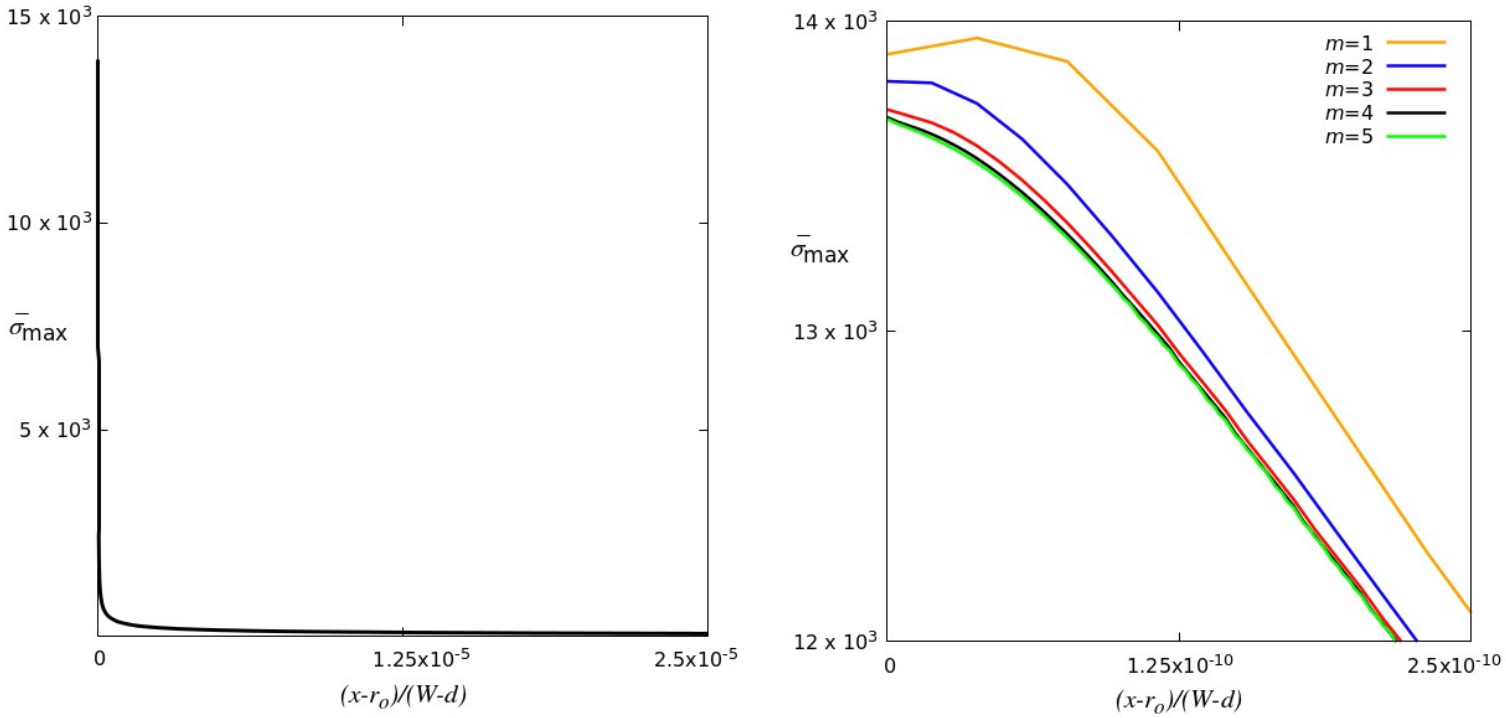

Fig. 5. (a) Normal stress along y=0 for r_o/δ=2.06, (b) detailed results near notch tip

To check for convergence, we let σ_m denote $\overline{\sigma}_{\max}$, and denote the increment accompanying mesh refinement as $\Delta\sigma_m=\sigma_m-\sigma_{m-1}$. We say that a mesh is converging if $\Delta\sigma_m$ is reducing for each mesh refinement and that $\Delta\sigma_m$ is the same sign. That is,

$$\begin{aligned}\Delta\sigma_m<\Delta\sigma_{m-1},\\ \Delta\sigma_m\times\Delta\sigma_{m-1}>1,\end{aligned} \tag{24}$$

must be true for convergence to occur. When the convergence criteria in Eq. (24) are satisfied for a given mesh and $m\geq2$, we calculate the estimated convergence rate using

$$\hat{c}_m=\ln\frac{\Delta\sigma_{m-1}}{\Delta\sigma_m}/\ln\lambda_m, \tag{25}$$

where $\lambda_m=N_m/N_{m-1}$. If the convergence criteria are satisfied and $m\geq3$, we calculate the estimated error (in percent) using

$$\hat{\varepsilon}_m = \frac{\Delta \sigma_m}{\sigma_m\left(\lambda_m^{\hat{c}_m} - 1\right)} \times 100. \tag{26}$$

For further details, see Ref. [6].

We apply the traction σ_o such that the peak stress at the notch root is within one percent of the ultimate stress, effectively determining the maximum stress concentration for a particular notch configuration. Table 4 shows the FEA results for r_o/δ=2.06 with uniform cohesive laws applied. Convergence does not occur initially, but the conditions in Eq. (24) are satisfied for m=4 and 5. In order to calculate $\Delta\sigma_m$ to three figures, we keep σ_m to seven figures. The error estimate is below our 1/5 percent threshold in m=4. However, we compute results for one finer mesh, m=5, as an assurance that the FEA continues to converge with further mesh refinement, and accept the result from m=5 as sufficiently accurately determined. This converged result is 99.2 percent of the ultimate stress.

Table 4. Finite element values of $\overline{\sigma}_{\max}$ with uniform cohesive laws for r_o/δ=2.06

m	σ_m	$\Delta\sigma_m$	$\hat{c}_m$	$\hat{\varepsilon}_m$ (%)
1	13893.18	-	-	-
2	13806.16	-87.02	-	-
3	13715.64	-90.52	-	-
4	13690.60	-25.04	1.85	0.07
5	13685.35	-5.25	2.25	0.01

Results for global meshes for other notch radii with cohesive laws active are given in Appendix C. These results consistently have converging error estimates that are below 1/5 percent, with one exception for r_o/δ=0, which approaches 1/5 percent.

As further verification of our FEA, we consider results from symmetry conditions and the TTP for r_o/δ=2.06. Table 5 contains the normalized maximum stress results from symmetry boundary conditions. An additional mesh, m=6, is used for the symmetry conditions and the TTP. This mesh contains 4,147,566 elements. From Table 5, we see the FEA begins to converge

from m=3 to m=4. The estimated error in m=6 is below 1/5 percent, and is therefore judged to be sufficiently accurately determined. We proceed to construct a TTP from this result.

Table 5. Finite element values of $\overline{\sigma}_{\max}$ with symmetry conditions for r_o/δ=2.06

m	σ_m	$\Delta\sigma_m$	$\hat{c}_m$	$\hat{\varepsilon}_m$ (%)
1	30,428.1	-	-	-
2	30,516.7	88.6	-	-
3	30,723.4	206.7	-	-
4	30,867.5	144.1	0.52	1.1
5	30,949.9	82.4	0.81	0.36
6	30,993.6	43.7	0.92	0.16

Using the results from the FEA, we determine the values specified in Eq. (19) and find the parameters in (20) to be

$$\alpha=4{,}962.5,\ \beta=2{,}260.0,\ \gamma=7{,}564.5, \tag{27}$$

with an exact value for $\overline{\sigma}_{\max}$=34,094, 10 percent higher than σ_6 in Table 5. The values in Eq. (27) are also exact and contain no additional figures. Using the parameters in Eq. (27) in the displacement fields given in Appendix B, we solve the same meshes as the originating FEA to determine the TTP results in Table 6. Table 6 also contains the true convergence rate and the true error, given as c_m and ε_m, respectively.

Table 6. Finite element values of $\overline{\sigma}_{\max}$ for the TTP with r_o/δ=2.06 (exact $\overline{\sigma}_{\max}$= 34,094)

m	σ_m	c_m	ε_m (%)	$\Delta\sigma_m$	$\hat{c}_m$	$\hat{\varepsilon}_m$ (%)
1	32,627.9	-	4.3	-	-	-
2	33,333.5	0.95	2.2	705.6	-	-
3	33,706.0	0.97	1.1	372.5	0.92	1.2
4	33,897.9	0.98	0.58	191.9	0.96	0.60
5	33,995.4	0.99	0.29	97.5	0.98	0.30
6	34,044.6	1.00	0.14	49.2	0.99	0.15

The results for the TTP in Table 6 begin to converge immediately. The true convergence rate c_m steadily approaches the asymptotic limit of 1 for 4Q elements as the mesh refines, eventually reaching 1.00 due to rounding. We accept the result from m=6 as being accurately determined. Where comparison may occur, the estimated error is conservative, but nonetheless tracks the true error well.

Both the FEA and TTP reach an estimated error below 1/5 percent. This TTP demonstrates that the mesh structure for this notch can accurately determine a peak stress that is much larger than that of Table 4. Therefore, we expect that the FEA with uniform cohesive laws is solved accurately as well.

Results for other TTP, specifically for the notches given by Eq. (12) are provided in Andrus and Sinclair [8]. The FEA and accompanying TTP for these notches consistently converge to an error level that is below 1/5 percent.

With the cohesive laws removed completely from the notch face, we obtain larger values of $\overline{\sigma}_{\max}$ than with uniformly applied cohesive laws. We select r_o/δ=0.00402 as the case to review results obtained with partially applied cohesive laws since this configuration produces the largest result for $\overline{\sigma}_{\max}$ obtained by FEA. Table 7 contains FEA results for r_o/δ=0.00402. Details for the mesh refinement sequence are given in Appendix A.

Table 7. Finite element values of $\overline{\sigma}_{\max}$ with cohesive laws removed from notch face for r_o/δ=0.00402

m	σ_m	$\Delta\sigma_m$	$\hat{c}_m$	$\hat{\varepsilon}_m$ (%)
1	35126.7	-	-	-
2	34333.0	-793.7	-	-
3	34127.4	-205.6	1.95	0.21
4	34075.1	-52.3	1.97	0.05

The FEA results in Table 7 begin to converge immediately. The result for m=4 is below the 1/5 percent threshold, and so we accept this result as sufficiently accurately determined.

Appendix D contains additional FEA results for the notch radii given by Eq. (13) with p=11–14. The FEA for each notch converges below the 1/5 percent threshold. We use the results in Appendix D to extrapolate a result for r_o/δ=0 of $\overline{\sigma}_{\max}$=34,170.8, which we judge to be sufficiently accurately determined. Appendix E contains details for the extrapolation procedure.

Regarding the physical implications of these results, we note that a different choice of material and cohesive laws will have some influence on the result. However, we expect that results for other similar materials and cohesive laws will produce a similar trend to the results here.

Figure 6 shows the results of $\overline{\sigma}_{\max}$ for each notch configuration given by Eqs. (12) and (13) with the various boundary conditions. It is readily apparent in Fig. 6(a) that for large radii, the cohesive laws yield the same results as the traditional symmetry conditions. Figure 6(b) shows results for the smaller radii of Eq. (13). The results with uniformly applied cohesive laws reach a finite value for the case of r_o/δ=0 and a maximum at r_o/δ=2. The results with the cohesive laws on only the symmetry plane are elevated compared to the uniform cohesive laws, but still finite. Figure 6(b) also indicates more clearly that peak stresses with traditional symmetry conditions are singular as the notch radius tends to zero.

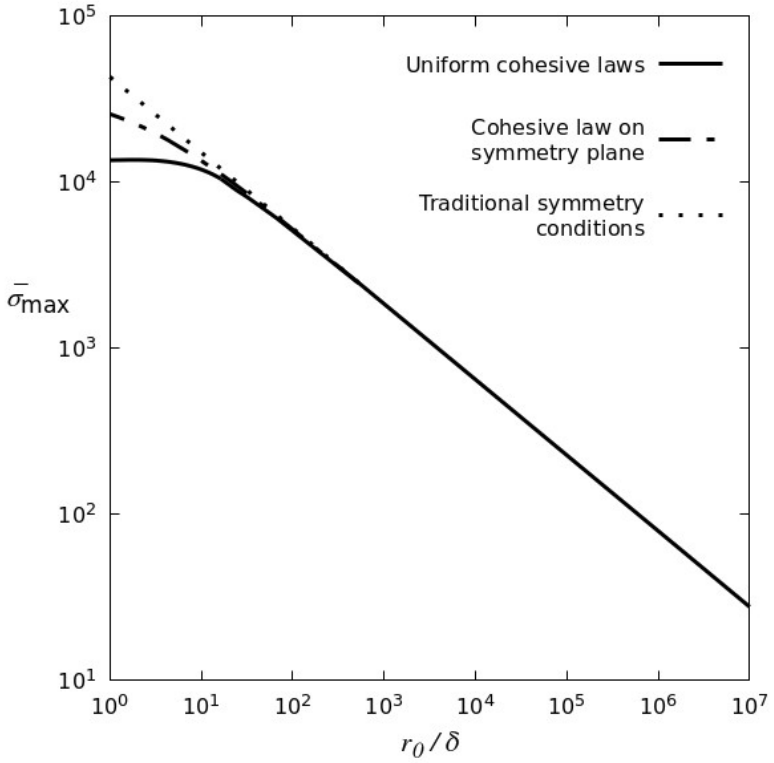

(a)

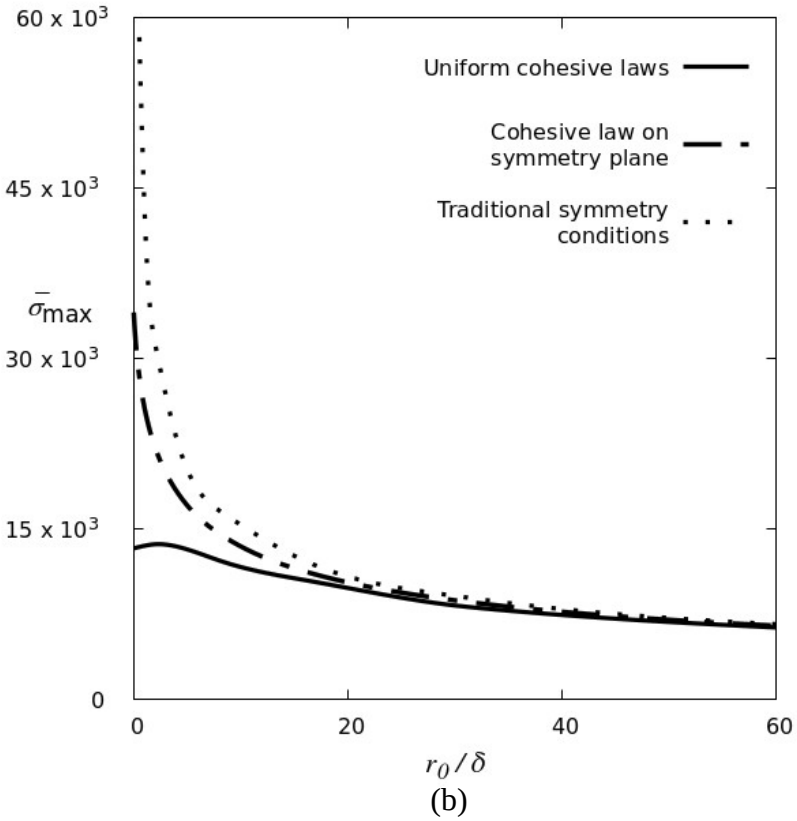

(b)

Fig. 6. Results for various notch acuities and boundary conditions: (a) overall results, (b) higher acuities

The results for $\overline{\sigma}_{\max}$ for traditional symmetry conditions agree well with the results for uniformly applied cohesive laws when r_o/δ is larger than approximately 500. For more acute radii, the results begin to deviate. When r_o/δ=66, the difference is within five percent. When r_o/δ=30, the difference is about 10 percent. When r_o/δ=2, where we obtain the largest normalized stress from uniformly applied cohesive laws, the difference is about 126 percent. It is evident that traditional symmetry conditions are applicable for a broad range of radii and the singular nature of the symmetry conditions is not pronounced until the notch is very acute.

The results for $\overline{\sigma}_{\max}$ for cohesive laws on the symmetry plane also agree with the results for uniformly applied laws for a broad range of radii. The difference between results for these boundary conditions is within one percent when r_o/δ=500. For a notch size of r_o/δ=30, the difference is within five percent. When r_o/δ=2, the difference is approximately 61 percent. For the sharp corner, r_o/δ=0, the difference between the results is approximately 156 percent.

In Table 8, we present the results for $\overline{\sigma}_{\max}$ for each boundary condition for the following notch configurations: r_o/δ=500, 30, 2, 0. We select r_o/δ=500 and 30 because these are the acuities where we see a negligible difference and a 10 percent difference, respectively, between symmetry conditions and cohesive laws. We pick r_o/δ=2 because we find the maximum $\overline{\sigma}_{\max}$ with cohesive laws at this notch acuity. Lastly, we select the sharp corner to present the finite stress results.

Table 8. Selected results for $\overline{\sigma}_{\max}$ with different boundary conditions

r_o/δ	Uniform cohesive laws	Partial cohesive laws	Traditional symmetry conditions
500	2,524	2,531	2,538
30	8,292	8,747	9,143
2	13,685	22,019	30,994
0	13,323	34,171	∞

5. Concluding Remarks

In this thesis, we consider a semi-infinite elastic plate with a 90-degree V-notch in one side and seek the peak stress at the notch tip as the notch radius approaches zero. As our principal focus, we seek results by implementing cohesive stress-separation laws on the notch face and symmetry plane between the upper and lower halves of the plate. We further seek results with cohesive laws applied only to the symmetry plane with stress free conditions on the notch face. Lastly, we consider results from traditional symmetry boundary conditions on the symmetry plane with stress-free conditions on the notch face.

We use FEA to conduct the analysis of these notch problems. We verify our FEA results with convergence checks and constructed test problems (TTP). This verification indicates that all reported results approach 1/5 percent accuracy or less.

The key conclusion from these results is that for a 90-degree V-notch with uniformly applied cohesive laws, the largest peak stress does not occur for the sharp corner, but rather for a notch radius of r_o/δ=2, where r_o is the local notch radius and δ is the equilibrium separation between atoms. We find this peak stress to be $\sigma_{\max}/\sigma_o = 13{,}700$, where $\sigma_{\max}$ is the peak stress at the notch tip and σ_o is an applied farfield traction. With the cohesive laws applied on only the symmetry plane, we find that as r_o tends to zero, peak stress results are larger than those with uniformly applied cohesive laws. For the partially applied laws, the peak stress result reaches a maximum of $\sigma_{\max}/\sigma_o = 34{,}100$ when r_o/δ=0, which is a sharp corner. Results from traditional symmetry conditions agree with the uniform cohesive laws for notch radii greater than r_o/δ=500. The results from symmetry conditions are about 10 percent higher than the uniform cohesive laws for a notch radius of r_o/δ=30.

Appendix A. Finite Element Meshes

Mesh structure for notches with greater acuity, such as those in Eq. (13), are shown in the text in Fig. 4. Notches with less acuity, as in Eq. (12), have a mesh structure that is illustrated in Fig. 7. The mesh in Fig. 7 is less refined since these notches have lower peak stresses at the notch root.

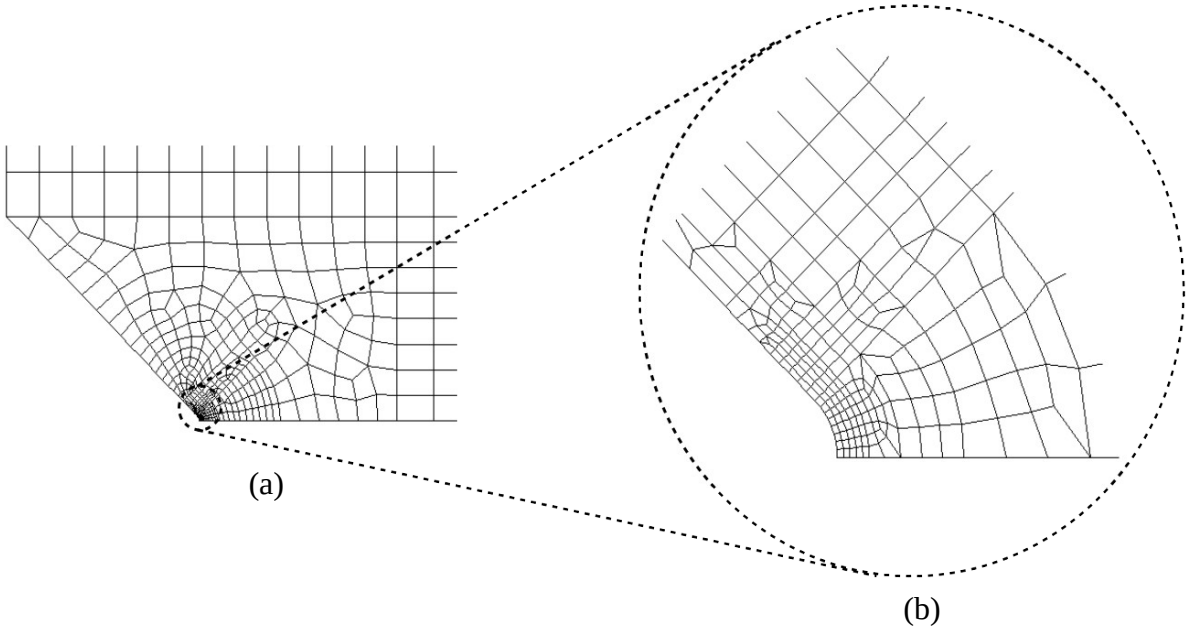

Fig. 7. Mesh m=1 for r_o/L=1/32: (a) farfield mesh, (b) detail near notch tip

Table 9 contains mesh sequences for these less refined meshes. To assess convergence, we use an element refinement factor of two. We halve element extents in the structured regions, strictly quadrupling elements in these regions. The element extent on the notch, h_m/r_o on $r=r_o$, for all of the configurations in Table 9 are 1/10.2, 1/20.4, 1/40.8, 1/81.6, 1/163. In the unstructured regions, we approximately quadruple the element counts, thus halving the element extents on average. This increases the overall number of elements N_m by close to a factor of four for each successive refinement, as seen in Table 9.

Table 9. Element numbers N_m for $r_o/L=0.5/16^n$

m	n=1	2	3	4	5
1	1,447	1,653	1,828	2,016	2,194
2	5,754	6,624	7,327	8,083	8,798
3	23,102	26,564	29,420	32,333	35,126
4	92,531	107,582	118,258	128,563	140,088
5	370,629	430,744	471,486	515,097	554,605
6	1,481,380	1,722,697	1,887,758	2,092,941	2,202,283

Table 10 contains the mesh sequences for the more refined meshes associated with the more acute notches of Eq. (13), excluding p=1, which is given in the text in Table 1. Again, N_m increases by close to a factor of four. The h_m/r_o is the same as in Table 1. Table 4 in the text provides FEA results for r_o/δ=2.06, when p=6, and includes a mesh m=5 with N_m=1,036,726 that is not given in Table 10.

Table 10. Element numbers N_m for $r_o/\delta=131.6/2^p$

m	p=2	3	4	5	6	7	8
1	3,647	3,743	3,845	3,948	4,049	4,144	4,241
2	14,563	14,985	15,412	15,762	16,169	16,591	16,791
3	58,273	59,873	61,454	63,055	64,734	66,324	67,927
4	232,835	239,321	245,713	252,079	259,141	265,504	271,893

For the FEA models with symmetry conditions and their corresponding TTP, the sequences in Table 10 include additional meshes, m=5, 6.

Table 11 contains the mesh sequences for the supplemental notches with r_o/δ=500 and 30. The mesh structure is similar to the notches in Table 10 with the same h_m/r_o as in Table 1.

Table 11. Element numbers N_m for supplemental r_o/δ

m	r_o/δ=500	30
1	3,250	3,647
2	12,958	14,582
3	51,924	58,317
4	207,148	207,149
5	828,573	-

Table 12 contains the mesh sequences for the additional notches used in the limiting case where the cohesive laws on the notch face are removed. The mesh structure is similar to the notches in Table 10, and again N_m increases by close to a factor of four. The h_m/r_o is the same as in Table 1.

Table 12. Element Numbers N_m for $r_o/\delta=131.6/2^p$

m	p=11	12	13	14	15
1	4,535	4,655	4,742	4,851	4,949
2	18,173	18,578	18,981	19,388	19,781
3	72,715	74,322	75,964	77,434	79,074
4	291,062	297,535	303,934	309,547	315,958

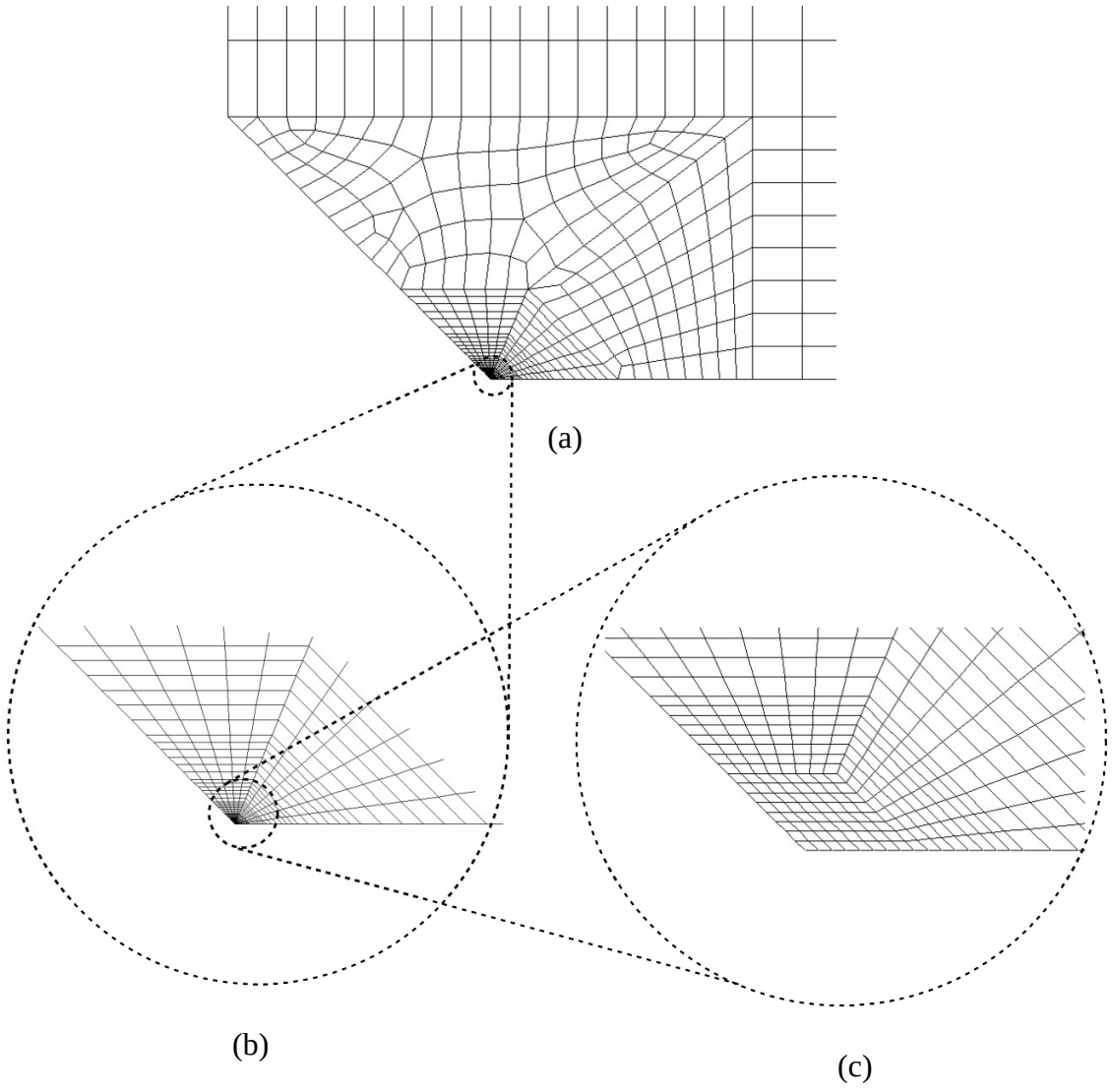

Fig. 8. Mesh m=1 for r_o/δ =0: (a) farfield, (b) structured mesh detail, (c) detail near notch tip

In Fig. 8, we show the mesh structure for sharp corner. We use a structured mesh near the tip of the V-notch that transitions with a free-meshed region into a structured mesh in the farfield.

Table 13 contains the mesh sequence for $r_o/\delta=0$. We use an element refinement factor of four, strictly quadrupling elements in the structured regions, and approximately quadrupling elements in the free-meshed transition region.

Table 13. Element numbers N_m for $r_o/\delta=0$

m	N_m
1	2,550
2	10,175
3	40,656
4	162,921
5	653,682

Appendix B. Fields for Tuned Test Problems

The following fields are from Ref. [7]. The stresses satisfy the stress equations of equilibrium and compatibility, and they have zero stress on $r=r_o$:

$$\sigma_r=\sigma_o\left[\alpha\left(1-\frac{r_o^2}{r^2}\right)-\beta\left(1+3\frac{r_o^4}{r^4}-4\frac{r_o^2}{r^2}\right)\cos 2\theta+\frac{\gamma r_o}{r}\left(1-\frac{r_o^2}{r^2}\right)\cos\theta\right],$$

$$\sigma_\theta=\sigma_o\left[\alpha\left(1+\frac{r_o^2}{r^2}\right)+\beta\left(1+3\frac{r_o^4}{r^4}\right)\cos 2\theta+\frac{\gamma r_o}{r}\left(1+\frac{r_o^2}{r^2}\right)\cos\theta\right],$$

$$\tau_{r\theta}=\sigma_o\left[\beta\left(1-3\frac{r_o^4}{r^4}+2\frac{r_o^2}{r^2}\right)\sin 2\theta+\frac{\gamma r_o}{r}\left(1-\frac{r_o^2}{r^2}\right)\sin\theta\right].$$

Their companion displacements satisfy the stress-displacement relations for a homogeneous, isotropic, linear, elastic solid in a state of plane strain:

$$u_r=\sigma_o\left[2\alpha\left((1-2\nu)r+\frac{r_o^2}{r}\right)-2\beta\left(r+4(1-\nu)\frac{r_o^2}{r}-\frac{r_o^4}{r^3}\right)\cos 2\theta\right.$$
$$\left.+\gamma r_0\left(\left(2(1-\nu)\ln\frac{r}{r_o}-1+\frac{r_o^2}{r^2}\right)\cos\theta+4(1-\nu)\theta\sin\theta\right)\right]/4\mu,$$

$$u_\theta=\sigma_o\left[2\beta\left(r+2(1-2\nu)\frac{r_o^2}{r}-\frac{r_o^4}{r^3}\right)\sin 2\theta\right.$$
$$\left.-\gamma r_0\left(\left(2(1-2\nu)\ln\frac{r}{r_o}+1-\frac{r_o^2}{r^2}\right)\sin\theta-4(1-\nu)\theta\cos\theta\right)\right]/4\mu.$$

Appendix C. Convergence Checks for Maximum Stresses with Uniform Cohesive Laws

The tables in this appendix provide detailed results from FEA with cohesive laws uniformly applied for the following notch configurations: $r_o/L=0.5/16^n$ for n=1, 3, 5, and $r_o/\delta=131.6/2^p$ for p=2, 4, 8. For the less acute notches, n=1, 3, 5, the results with cohesive laws are the same as with traditional symmetry conditions. Tables 14–16 contain results for the less acute notches where n=1, 3, 5, and Tables 17–19 contain results for the more acute notches where p=2, 4, and 8. Table 20 includes the result for r_o/δ=0.

Table 14. Finite element values of $\overline{\sigma}_{\max}$ for r_o/L= 0.5/16

m	σ_m	$\Delta\sigma_m$	$\hat{c}_m$	$\hat{\varepsilon}_m$ (%)
1	15.1121	-	-	-
2	15.4496	0.3375	-	-
3	15.6313	0.1817	0.89	1.4
4	15.7239	0.0926	0.97	0.61
5	15.7708	0.0469	0.98	0.31
6	15.7945	0.0237	0.99	0.15

Table 15. Finite element values of $\overline{\sigma}_{\max}$ for r_o/L= 0.5/16^3

m	σ_m	$\Delta\sigma_m$	$\hat{c}_m$	$\hat{\varepsilon}_m$ (%)
1	190.074	-	-	-
2	194.013	3.939	-	-
3	196.246	2.233	0.82	1.5
4	197.393	1.147	0.96	0.61
5	197.980	0.587	0.96	0.31
6	198.274	0.294	1.00	0.15

Table 16. Finite element values of $\overline{\sigma}_{\max}$ for r_o/L= 0.5/16^5

m	σ_m	$\Delta\sigma_m$	$\hat{c}_m$	$\hat{\varepsilon}_m$ (%)
1	2366.77	-	-	-
2	2418.73	51.96	-	-
3	2447.27	28.54	0.86	1.4
4	2461.44	14.17	1.01	0.57
5	2468.54	7.10	1.00	0.29
6	2472.01	3.47	1.04	0.13

Table 17. Finite element values of $\overline{\sigma}_{\max}$ for r_o/δ=32.9

m	σ_m	$\Delta\sigma_m$	$\hat{c}_m$	$\hat{\varepsilon}_m$ (%)
1	8206.82	-	-	-
2	8062.87	-143.95	-	-
3	8025.36	-37.51	1.94	0.16
4	8017.96	-7.40	2.34	0.02

Table 18. Finite element values of $\overline{\sigma}_{\max}$ for r_o/δ=8.23

m	σ_m	$\Delta\sigma_m$	$\hat{c}_m$	$\hat{\varepsilon}_m$ (%)
1	12540.3	-	-	-
2	12266.4	-273.9	-	-
3	12190.1	-76.3	1.85	0.24
4	12175.8	-14.3	2.42	0.12*

Table 19. Finite element values of $\overline{\sigma}_{\max}$ for r_o/δ=0.514

m	σ_m	$\Delta\sigma_m$	$\hat{c}_m$	$\hat{\varepsilon}_m$ (%)
1	13547.92	-	-	-
2	13534.43	-13.49	-	-
3	13492.41	-42.02	-	-
4	13454.29	-38.12	0.14	2.77
5	13444.90	-9.39	2.02	0.07*

Table 20. Finite element values of $\overline{\sigma}_{\max}$ for r_o/δ=0

m	σ_m	$\Delta\sigma_m$	$\hat{c}_m$	$\hat{\varepsilon}_m$ (%)
1	14760.1	-	-	-
2	14007.4	-752.7	-	-
3	13564.4	-443.0	-	-
4	13383.7	-180.7	1.29	0.93
5	13323.0	-60.7	1.57	0.23

Results for estimated errors in Tables 14–19 consistently converge below 1/5 percent. Results for intermediary notch sizes likewise converge with estimated errors below 1/5 percent. The result in Table 20 for r_o/δ=0 approaches an estimated error of 1/5 percent. The results denoted with an asterisk are calculated by taking $\hat{c}_m$=1.0 to avoid significantly underestimating the error when the convergence rates increase significantly: this is done in accordance with the modified convergence estimates of Beisheim et al. [9].

Appendix D. Convergence Checks for Maximum Stresses with Cohesive Laws on Symmetry Plane

The tables in this appendix provide detailed results from FEA with cohesive laws applied to only the symmetry plane for the following notch configurations: $r_o/\delta=131.6/2^p$ for p=11, 12, 13, 14. Tables 21–24 provide results for these notches in order of increasing notch acuity.

Table 21. Finite element values of $\overline{\sigma}_{\max}$ for r_o/δ=0.0643

m	σ_m	$\Delta\sigma_m$	$\hat{c}_m$	$\hat{\varepsilon}_m$ (%)
1	34067.2	-	-	-
2	33251.0	-816.2	-	-
3	33044.3	-206.7	1.98	0.63
4	32989.8	-54.5	1.92	0.17

Table 22. Finite element values of $\overline{\sigma}_{\max}$ for r_o/δ=0.0321

m	σ_m	$\Delta\sigma_m$	$\hat{c}_m$	$\hat{\varepsilon}_m$ (%)
1	34563.9	-	-	-
2	33780.6	-783.3	-	-
3	33573.8	-206.8	1.92	0.22
4	33520.0	-53.8	1.94	0.06

Table 23. Finite element values of $\overline{\sigma}_{\max}$ for r_o/δ=0.0161

m	σ_m	$\Delta\sigma_m$	$\hat{c}_m$	$\hat{\varepsilon}_m$ (%)
1	34871.8	-	-	-
2	34081.9	-789.9	-	-
3	33873.0	-208.9	1.92	0.22
4	33820.2	-52.8	1.98	0.05

Table 24. Finite element values of $\overline{\sigma}_{\max}$ for r_o/δ=0.00803

m	σ_m	$\Delta\sigma_m$	$\hat{c}_m$	$\hat{\varepsilon}_m$ (%)
1	35030.6	-	-	-
2	34244.6	-786.0	-	-
3	34038.0	-206.6	1.93	0.22
4	33985.4	-52.6	1.97	0.05

Each FEA converges below the 1/5 percent threshold when m=4, so we accept these results as being sufficiently accurately determined.

Appendix E. Peak Stress Results with r_o=0 with Cohesive Laws on the Symmetry Plane

Determining a consistent result through FEA for r_o/δ=0 with the cohesive laws removed from the notch face proved challenging due to implementation of the COMBIN39 spring element at the sharp corner. When the notch has a nonzero radius, we obtain consistent results through FEA with the spring elements removed from the notch face, and so choose to extrapolate a result for r_o/δ=0.

We create increasingly acute notches beyond those given in the text with Eq. (13) to include notch configurations for p=11, 12, …, 15. The smallest notch configuration created with cohesive laws removed from the notch face is r_o/δ=0.00402. We use converged results from these notches for our extrapolation procedure, shown next.

Extrapolation proceeds with

$$K = K_o - \Delta K_1 \left(\frac{R}{r_o}\right) + \Delta K_2 \left(\frac{R}{r_o}\right)^2 - \Delta K_3 \left(\frac{R}{r_o}\right)^3, \tag{28}$$

where K_o, ΔK_1, ΔK_2, and ΔK_3 are constants, $K = \overline{\sigma}_{\max}$ and is determined with FEA, R is the corresponding notch radius for an accompanying K, and r_o is a reference radius. We test this method by extrapolating a result for r_o/δ=0.00402 and comparing it to the FEA result.

Table 25 shows the results for $\overline{\sigma}_{\max}$ from the finest mesh of each notch for p=11–15.

Table 25. Finite element results for $r_o/\delta = 131.6/2^p$ with partially applied cohesive laws and p=11, 12, … , 15

$r_o/\delta = 131.6/2^p$	$\overline{\sigma}_{\max}$
p=11	32,989.8
12	33,520.0
13	33,820.2
14	33,985.4
15	34,075.1

Each increase of p causes r_o to decrease by exactly half, so taking the results for p=11–15 from Table 25, we solve the following system of equations:

$$32{,}989.8 = K_o - \Delta K_1 + \Delta K_2 - \Delta K_3, \tag{29}$$

$$33{,}520.0 = K_o - \frac{\Delta K_1}{2} + \frac{\Delta K_2}{4} - \frac{\Delta K_3}{8}, \tag{30}$$

$$33{,}820.2 = K_o - \frac{\Delta K_1}{4} + \frac{\Delta K_2}{16} - \frac{\Delta K_3}{64}, \tag{31}$$

$$33{,}985.4 = K_o - \frac{\Delta K_1}{8} + \frac{\Delta K_2}{64} - \frac{\Delta K_3}{512}, \tag{32}$$

and find $K_o = 34{,}163.07619$, $\Delta K_1 = 1{,}476.133333$, $\Delta K_2 = 457.0666667$, and $\Delta K_3 = 154.2095238$. Substituting the foregoing results into Eq. (28), we determine K=34,072.6 for r_o/δ=0.00402, which is within 0.01 percent of the FEA result in Table 7. Thus, we conclude that the extrapolation procedure works well and use it to determine a result for r_o/δ=0.

References

[1] Williams, M. L., 1952, “Stress Singularities Resulting from Various Boundary Conditions in Angular Corners of Plates in Extension,” ASME J. Appl. Mech., **19**, pp. 526-528.

[2] Sinclair, G. B., 1996, “On the Influence of Cohesive Stress-Separation Laws on Elastic Stress Singularities,” J. Elasticity, **44**, pp. 203-221.

[3] Sinclair, G. B., Meda, G., and Smallwood, B. S., 2011, “On Crack-Tip Stresses as Crack-Tip Radii Decrease,” ASME J. Appl. Mech., **78**, p. 011004.

[4] Cherepanov, G. P., 1979, *Mechanics of Brittle Fracture,* McGraw-Hill, New York.

[5] ANSYS, 2018, “ANSYS Mechanical APDL Element Reference,” Release 19.1, ANSYS Inc., Canonsburg, PA.

[6] Sinclair, G. B., Beisheim, J. R., and Roache, P. J., 2016, “Effective Convergence Checks for Verifying Finite Element Stresses at Two-Dimensional Stress Concentrations,” ASME J. Verif. Valid. Uncert. Quant., **1**, p. 041003.

[7] Sinclair, G. B., Anaya-Dufresne, M., Meda, G., and Okajima, M., 1998, “Tuned Test Problems for Numerical Methods in Engineering,” Int. J. Numer. Methods Eng., **40**, pp. 4183-4209.

[8] Andrus, T. M., and Sinclair, G. B., 2020, “Verification of Finite Element Analysis for the Stress Concentrations Occurring at V-Shaped Notches Using Tuned Test Problems,” Report No. ME-MS2-20, Department of Mechanical Engineering, Louisiana State University.

[9] Beisheim, J. R., Sinclair, G. B., and Bilich, L. A., 2015, “Convergence Checks in the Presence of Nonmonotonic Convergence,” Proc. NAFEMS World Congress, San Diego, CA, on CD-ROM.

Vita

Trent Andrus was born and raised in Lafayette, Louisiana. Trent attended Louisiana State University for his Bachelor of Science in Mechanical Engineering and graduated in 2018 with Upper Division Honors Distinction from the Roger Hadfield Ogden Honors College. While at LSU for his undergraduate degree, Trent participated in the SpaceX Hyperloop Design Competition, founded a student organization focused on environmental issues, and completed a photo-documentary project entitled *Louisiana Gone* with a colleague using funds from the Roger Hadfield Ogden Honors College. *Louisiana Gone* was entered in the 2017 LSU Discover Day Juried Art Show, where it was awarded "Tiger's Choice" as a fan-favorite. Trent continued his education at LSU, beginning a Master of Science for Mechanical Engineering in 2018 and anticipates graduation in Fall 2020. Trent conducted research using finite element analysis software for his undergraduate and graduate degrees. During his Master's, Trent interned at Ansys, where he now works full-time as a R&D Verification Engineer.